Journal of Thermal Analysis and Calorimetry, Vol. 76 (2004) 693–708

OPTIMISING OF THE SENSING CHAMBER OF AN ARRAY OF A VOLATILE DETECTION SYSTEM
Fluid dynamic simulation

S. M. Scott, D. James, Z. Ali and W. T. O'Hare*

School of Science and Technology, University of Teesside, Middlesbrough, TS1 3BA, UK

Abstract

A fluid dynamic analysis was performed to optimise the positioning of sensor elements in a coated quartz crystal microbalance (QCM) based volatile detection system. The computational fluid dynamic (CFD) code used solves the Navier–Stokes equations statically and dynamically in 2D, discretised by finite elements. In the original sensor chamber, the sensor elements were positioned in a staggered pattern and at 90° to the incoming flow. The numerical analysis shows that, with the exception of the front face of the first sensor, only 45% of the flow passed over the sensors. It is shown that the response of sensor elements is strongly dependent on the sensor position. An optimised sensor chamber design was developed where the sensors are at 0° to the flow direction and a baffle plate diffuses the flow evenly over the sensor elements. The sensors are shown to receive the same flow and respond identically irrespective of position.

Keywords: CFD, gas, optimisation, piezoelectric, QCM, sensor

Introduction

Electronic noses (EN) are based on an array of semi-selective chemical sensors used to analyse headspace volatiles and odours. Many different types of gas sensor have been used for EN applications [1–3]. Coated QCMs are attractive since changing the applied coating may alter their sensing properties. The array responses are analysed by a pattern recognition technique, which provides the selectivity required for identification of the volatile. This action mimics biological olfaction in which the brain carries out the identification of responses from the olfactory receptors. The major purpose of ENs is to provide rapid inexpensive headspace analysis of volatile organic compounds without the use of skilled technicians, who are required for other headspace analysis techniques such as GC-MS.

The EN system generally consists of a sampling method in which the headspace volatiles to be analysed are generated and brought to the sensor chamber. The sensors will respond to the odour producing a data pattern that may be analysed for classification of the volatile. Many different [4, 5] sample generation systems have been used in

* Author for correspondence: E-mail: z.ali@tees.ac.uk

1388–6150/2004/ $ 20.00

Akadémiai Kiadó, Budapest
Kluwer Academic Publishers, Dordrecht

attempts to produce more intuitive data including static, dynamic, injection and preconcentration. McAlernon *et al.* [6] used a commercial EN to investigate the effect of two different sample generation chamber dimensions and sample volumes. The first involved 10 mL of sample being placed into a 60 mL glass jar and allowed to equilibrate at 25°C for 10 min. The second consisted of a 0.5 mL sample in a 1.5 mL polypropylene vial at 25°C. The same recirculation sampling regime was utilised for both sample chambers. It was found that the acquired data from the two chambers differed significantly at 95% confidence intervals. For readings relying upon overall response magnitude for successful classification, the vial method performed best. The jar method gave higher overall headspace responses but more scatter and provided better classification if the gradients of response were used as the analyte predicator. They concluded that the kinetic signatures provided valuable information; this infers that an array of sensors should all be exposed simultaneously to the analyte.

A preconcentration tube based sampling regime for the detection of toluene in water was investigated by Ali *et al.* [7] and found that an EN could detect toluene reproducibly at concentrations as low as 0.01% in water.

A large number of publications have also concentrated specifically on pattern recognition methods to improve upon the identification made by the EN responses [8–9]. Holmberg *et al.* [10] tried with some success to utilise two different pattern recognition methods to counteract the effect of sensor drift on odour classifications. It was found that a self-organizing classifier and a method which models the sensors as a dynamic system, relying upon correlation between signals from different sensors, gave considerably better results than a standard back-propagation (BP) neural network. Ali *et al*. [11] discriminated between different fresh edible oils using Radial Basis Function (RBF) neural networks, James *et al*. [12] used fuzzy *c*-means. It was possible in both cases to discriminate between sunflower, olive and extra virgin olive oil by their headspace profile.

Little work has been published on the design and dynamics of the sensor chamber. Falcitelli *et al*. [13] carried out a fluid dynamic simulation of the sensor chamber of a commercial EN using conducting polymer sensors in a planar configuration. Their work investigated the optimisation of sensor signals, for a constant concentration of the species odour. Falcitelli's study was entirely theoretical in its approach, using CFD only.

This study investigates the optimisation of QCM sensor signals due to sensor chamber design using CFD verified by flow visualisation and measured sensor responses.

Design criteria

The sensor chamber needs to be systematically designed; materials need to be selected that are tough but machinable, chemically inert and non-adsorbent to avoid memory effects. The heat sink properties of the chamber could also be important for temperature control of the analyte to avoid condensation and its related problems. The chamber geometry should be arranged so that there are no recirculating zones within the operating flow rate range, the chamber volume kept to a minimum for

rapid refresh rate. The optimum flow rate needs to be determined for the sampling regime used so that the sensors are exposed to the analyte for a sufficient residence time to sorb into the sensor coating but not so that the analyte headspace is diluted. The optimum flow angle over the sensors should be determined and accommodated in the design. All sensors should be exposed simultaneously to a homogeneous flow of species to prevent position related performance.

Material choice

Good choices of material are stainless steel and polytetrafluoroethylene (PTFE). Stainless steel is strong (up to 1800 MPa), tough, has good thermal conductivity (26 W m^{-1} °C^{-1}), is inert and non-absorbent but does work harden during machining. PTFE is reasonably tough, flexible, useful up to a maximum temperature of 260°C, has poor thermal conductivity (0.27 W m^{-1} °C^{-1}) and is inert, but is microporous, so the exposed surface area of PTFE to the analyte needs to be kept to a minimum and care taken in use to properly desorb any odorous materials between samples.

Flow characteristics

The flow of viscous fluids is usually characterised by several dimensionless ratios; for pressure driven flow the Reynolds number (*Re*) is the most important. The Reynolds number is a measure of the kinetic forces to the viscous forces in a flowing fluid and is defined as, $Re=\rho dU/\mu$, where ρ is the density of the fluid (kg m^3), *d* is the hydraulic diameter (*m*); *U* is the fluid mean velocity (*m*/s) and μ is the dynamic viscosity of the fluid (kg ms^{-1} or Ns m^{-2}). The three types of flow characterised by ranges of Reynolds numbers are shown in Table 1.

Table 1 Reynolds number and type of flow

Reynolds number range	Type of flow
RE < 2300	Laminar flow
2300 <= *Re* < 4000	Transitional flow
Re = 4000	Turbulent flow

Computational fluid dynamics (CFD)

CFD solutions are based on the Navier–Stokes equations and require that a model be created accurately reflecting the geometry of the system. Within the fluid subdomain the properties of the fluid need to be specified. A discretisaton of the model is performed, boundary conditions set, and then a solution may be found via an iterative solver. Course meshes may not converge, fine meshes may take large amounts of memory and CPU time to solve, in general the finer the mesh the more accurate the solution. Both two and three-dimensional models may be used, two-dimensional ones are quicker to build and solve but will not show 3D effects.

Numerical modelling

Modelling of dynamic fluid systems is performed numerically using the Navier–Stokes equations which are very difficult to solve, even with modern digital computers. The basic equations are considered here to be the three laws of conservation for physical systems.

1. Conservation of mass (continuity)
2. Conservation of momentum (Newton's second law)
3. Conservation of energy (first law of thermodynamics)

The above are complete if there is only one homogeneous fluid. If any of the following are true then there are at least two more considerations, the fluid is non-homogeneous, there is diffusion, chemical-reaction or multi-component reacting fluids:

4. Conservation of species
5. Chemical reaction equations

If only homogeneous basic flow in three dimensions (*x, y, z*) with the velocity components **V**=(*u, v, w*) is considered, then the Navier–Stokes equations may be written as a single vector equation using the indicial notation.

$$\rho\frac{D\mathbf{V}}{DT}=\rho\mathbf{g}-\nabla p+\frac{\partial}{\partial x_j}\left[\mu\left(\frac{\partial v_i}{\partial x_j}+\frac{\partial v_j}{\partial x_i}\right)+\delta_{ij}\lambda\mathrm{div}\mathbf{V}\right] \quad (1)$$

If the fluid is assumed to be of constant density, div**V** disappears from the continuity equation and the vexing coefficient λ disappears from Newton's law. If the viscosity μ is assumed constant, many terms vanish, leaving a simple form of the Navier–Stokes equation for constant viscosity and density.

$$\rho\frac{D\mathbf{V}}{Dt}=\rho\mathbf{g}-\nabla p+\mu\nabla^2\mathbf{V} \quad (2)$$

This equation may perform poorly for non-isothermal flows, particularly for liquids whose viscosity is highly temperature dependent.

Matlab 6.5.1 [R13sp1] (Mathworks UK) with Femlab 2.3b (Comsol UK) were used to model the systems. Femlab uses a finite element discretisation and is able to solve both static and dynamic solutions. The Navier–Stokes module was used for the static flow analysis of the chambers.

Diffusion of species

Determination of the dynamic concentration may be achieved by consideration of the flow and factoring in the diffusion of the species. The Navier–Stokes coupled to the Convection and Diffusion modules were used for the dynamic concentration analysis. The coupling of the modules is known as multiphysics and is achieved in this case by determining the instantaneous *u* and *v* velocities of the flow from the Navier–Stokes

equations and using these values in the Convection and Diffusion calculations. If c is a concentration, D a diffusion coefficient and Q a volume source, then:

$$\frac{\partial c}{\partial t} - \nabla(D\nabla c) = Q$$

Sensors

The sensors are made from α-quartz, a crystallographic system that exhibits piezoelectricity. This effect is utilised using gold electrodes attached to the quartz and exerting an alternating current that results in the crystal oscillating with a fundamental frequency. The QCMs used were AT cut (35°15' inclination in the y–z plane) with 5 mm diameter circular polished gold electrodes on both sides of 1000 Å thickness bonded onto a chromium 100 Å thickness substrate on an 8 mm square quartz wafer connected to a HC49/U holder (International Crystal Mfg. Co. Inc. Ok, USA). Any layer added to the crystal, which does not dampen the oscillation, may be treated as added thickness, causing a change in frequency that is proportional to the change in mass. A diagram of a QCM sensor can be seen in Fig. 1. QCMs act as sensors by the immobilisation of a chemical or biochemical layer on the device surface. The chemical or biochemical layer is used to abstract analyte from the sample stream to the device surface. The Sauerbrey [14] Eq. (3) demonstrates that the change in device frequency is proportional to the mass of material sorbed (adsorption or absorption) by the coating layer on the crystal surface.

$$\Delta f = 2.3 \cdot 10^6 f_0^2 \frac{\Delta M_s}{A} \tag{3}$$

where Δf is the change in frequency of the QCM (Hz), f_0 is the resonant frequency of the quartz crystal (MHz), ΔM_s is the mass of the coating or substance sorbed (g) and A is the area coated (cm^2).

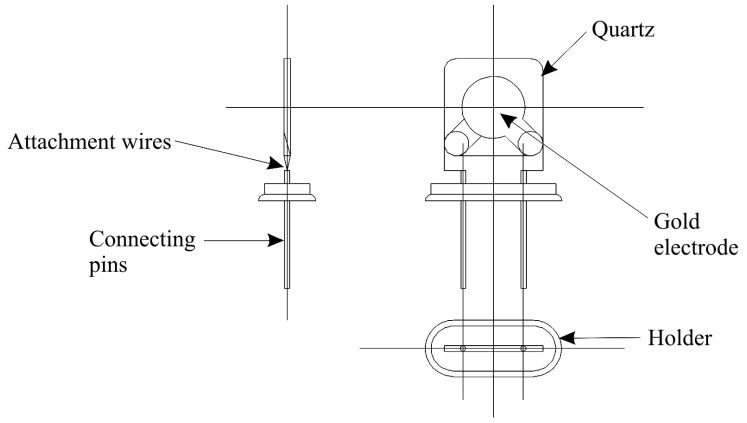

Fig. 1 QCM sensor

Sensor response

Figure 2 shows a typical sensor frequency response to the step change in concentration of species from a zero to an arbitrary constant concentration at an arbitrary time equals zero. The response curves approximate to an open loop first order response. The actual equation for the sensor response is described by Freeman [15] as the sum of two exponentials and given by Eq. (4).

$$\Delta f(t) = a_1(1-e^{-a_2 t}) + a_3(1-e^{-a_4 t}) \quad (4)$$

where a_1 to a_4 are constants and t is time (s). The values of terms a_1 and a_3 depend on the mass of the sensor coating and the analyte sorbed, ΔM_s, from Eq. (3). The value of terms a_2 and a_4 depend on the dynamic interaction of the sensor coating and the analyte, they give the shape of the response curve. The first term is thought to be a bulk response (absorption) and accounts for approximately 90% of the total; the second is due to surface effects (adsorption) and accounts for the remaining 10% of the total.

The aim of the design process is to ensure that the entire incoming sample stream is distributed rapidly, simultaneously and evenly over all of the sensors under the same conditions.

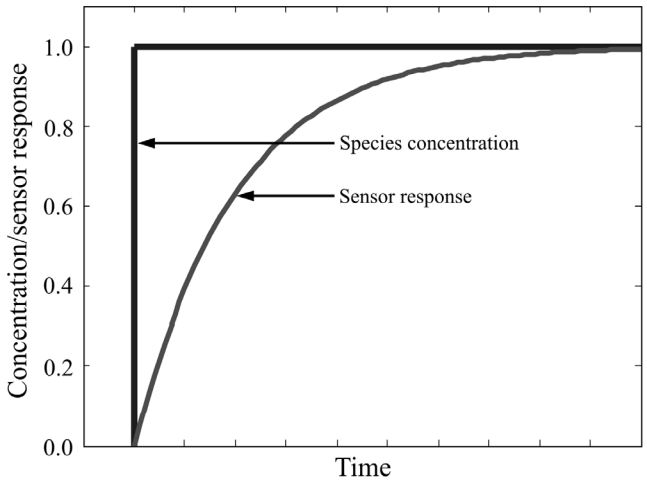

Fig. 2 Sensor response

Original sensor chamber

The original sensor chamber, as shown in Fig. 3, was from a previous study; it was constructed from PTFE and is rectangular, 40 mm in length, 19 mm in width and 15 mm in height. The sensors are at 90° to flow, spaced a 6 mm intervals, an alternating offset from the centreline of 5 mm creates a staggered pattern. The inlet and

outlet holes for the gas flow are 3 mm in diameter, centred 8 mm above the base of the sensors so the gas flow is approximately centred on the sensing plane. A reference QCM is located externally to the chamber. The chamber was modified for flow visualisation by machining to fit Perspex top and bottom covers, held in place with bolts, the joints sealed by 48 mm diameter nitrile 'O' rings.

Flow cell

The test flow cell is constructed from stainless steel and PTFE and consists of a circular chamber 20 mm in diameter, 15 mm in height, the 3 mm inlet and outlet holes are 5 mm above the base of the sensors so that gas inlet and outlet are approximately

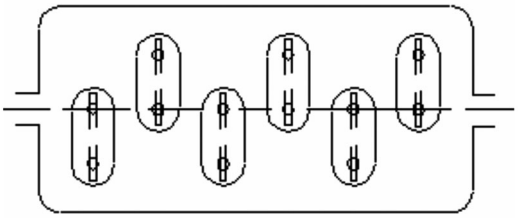

Fig. 3 Original sensor chamber

central to the sensing area of the QCM. The chamber body block is stainless steel and is rotatable about locating stub on the base (PTFE) by 110° so that the flow angle may be changed relative to the sensor orientation. A removable baffle plate (stainless steel) may be used to diffuse the incoming gas before passing over the sensors. There are holes in the base stub to accurately locate the sensors and allow for electrical connection to the oscillating circuitry and data acquisition hardware. The small surface area of the base exposed in the chamber minimises the possible memory effect of the PTFE. There are two sensors internal to the chamber; the central QCM is used as a reference. Two top covers were used, stainless steel for normal use and Perspex for flow visualisation. A nitrile 'O' ring between the top cover and body and a shaft seal between the body and base seal the unit.

Sensor coating

The QCMs were coated using Diethylene glycol succinate (DEGS), (Phase Separations Ltd, Deeside, UK). The coating solution was prepared by diluting 3 g of DEGS with 97 g of dichloromethane, resulting in a 3 mass/mass% solution. A further 10 times dilution was then carried out to give a 0.3 mass/mass% coating solution. The QCMs were initially cleaned with methanol, followed by dichloromethane and then rinsed with double distilled water. Coatings were applied by a 0.2 μL drop of solution from a Hamilton GC syringe (Alltech, Lancs, UK). During this process the resonant frequency was monitored by a Fluke PM6685 universal frequency counter (Fluke U.K. Ltd, Watford, UK) to ensure similar frequency shifts (coating mass) of the QCMs. The

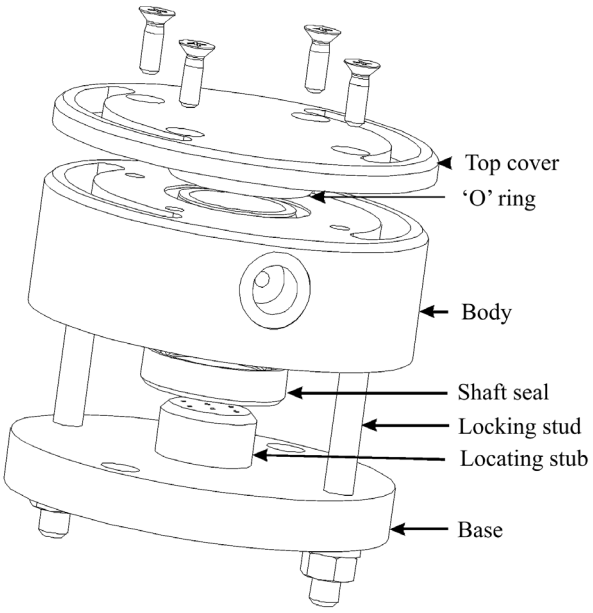

Fig. 4 Test flow cell assembly

sensors were then immediately placed into the EN chamber and conditioned by passing nitrogen over them for 6 h.

Experimental technique of sensor responses for flow rate

A 250 cm^3 glass bottle (Omnifit, UK) containing 10 mL of toluene was stored in a water bath at 27°C for 30 min to allow headspace generation. Dynamic headspace analysis with a flow angle of 90° was carried out by passing a nitrogen stream through the sample bottle into the flow chamber. A four-way PTFE valve allowed the sample or reference nitrogen gas stream to be alternated through the chamber for either sampling or purging. The flow rate for both streams was set at 40 mL min^{-1} by mass flow controllers (Brooks 5850S thermal mass flow controller). Sampling was performed over a 3 min cycle, 1 min to obtain a base line reference and 2 min for the sensor response (sample). After each sample run the flow chamber was purged with nitrogen for 2 min before repeating the cycle. Twenty readings were taken for each sample, and then the flow rate altered and repeated. Flow rates from 40 to 120 mL min^{-1} with 10 mL min^{-1} intervals were taken.

Flow angle

Sampling was performed for flow angles from 90 to 0° at 10° intervals at a flow rate of 40 mL min^{-1}.

Visualisation

The flow visualisation apparatus is shown in Fig. 5 and consisted of a smoke generation chamber in which mineral oil was heated to a vapour by a nichrome wire coil powered by a variable current DC supply. Smoke (oil vapour) was driven from the generation chamber and through the sensor chamber by a nitrogen stream regulated by a mass flow controller. The mass flow controller was itself controlled via a digital microprocessor control and readout unit (Brooks 0154) connected to an Intel Celeron 333 PC via a RS232 interface to control software (Brooks Smart DDE V1.2 and Testpoint application software). A digital camera (TK-1280E video camera with a Computar 1:1.5 TV lens) sent an image stream to the PC via a video capture card (Matrox Meteor) for processing and storage by software (Matrox Inspector 2.1). A moveable light source was used to illuminate the chamber.

Experimental technique

Smoke was passed through the flow chamber at 60 mL min^{-1}, images were captured at 20 ms intervals and saved as an audio video interleave (avi) file. The original chamber, the flow cell with sensors at 90, 0 and 0° with a baffle plate were tested. The captured images were compared with the static and dynamic CFD results.

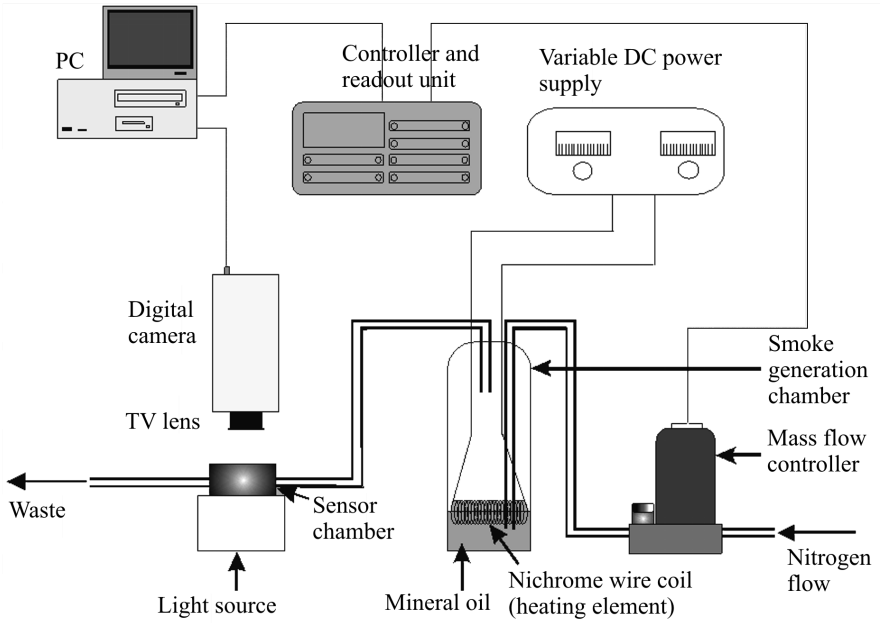

Fig. 5 Flow visualisation experimental apparatus

Results

Flow rate

Figure 6 shows the effect of varying flow rates on the sensors in the 90° configuration. Averages of twenty readings are shown with error bars added. High flow rates affect the front sensor far more than the rear sensor. The mid flow rate region shows less variation than the extremes. A flow rate of 60 mL min^{-1} allows for the sensor chamber to be refreshed every 5 s whilst not depleting the generated headspace, which is often the case with the higher flow rates where the concentration of species is reduced. The best compromise flow rate was 60 mL min^{-1}.

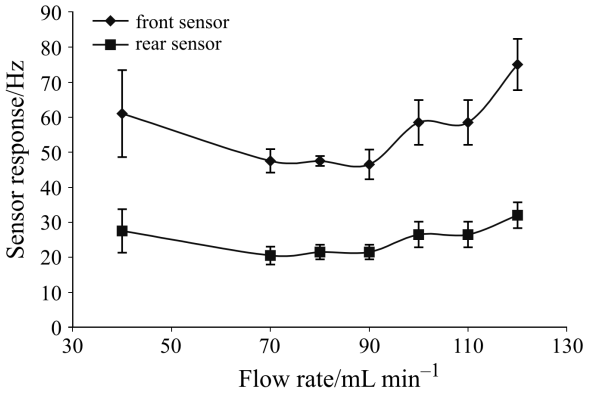

Fig. 6 Flow rate responses for sensors at 90° to flow in flow cell (no baffle)

Flow angle results

Table 2 shows the properties of nitrogen used in the numerical analysis, *D* is the mass diffusion for oil smoke in nitrogen, *Sc* is the Schmitt number which is a measure of viscous diffusion to mass diffusion.

Table 2 Nitrogen properties

Property	Symbol (unit)	Value
Density	ρ/kg m^{-3}	1.25
Dynamic viscosity	μ/kg ms^{-1}	$1.8e^{-5}$
Diffusion coefficient	*D*/m^2 s^{-1}	$1.5e^{-7}$
Kinematic viscosity	*v*=μ/ /m^2 s^{-1}	$1.44e^{-5}$
Schmitt number	*Sc*=*v*/D(–)	97

The flow through the chamber over the sensing area of the QCMs may be reasonably approximated in 2D. A 2D model is effectively a slice through the

centreline of the flow where the sensing takes place; 3D effects have little relevance. All simulations were modelled in 2D at constant temperatures. The original flow cell was modelled in full, whilst only half of the test cell was modelled due to symmetry. A flow rate of 60 mL min^{-1} in the 3 mm inlet tube gives a mean velocity U of 0.141 m s^{-1} and a Reynolds number of 29.5. This flow is laminar (Hagen–Poiseuille), typical for electronic nose devices.

For Hagen–Poiseuille flow at inlet $U=Q/A$, where Q is the volumetric flow rate and A is the cross sectional area.

$$U=\frac{1}{2}u_{\max}=\frac{Q}{A} \tag{5}$$

The velocity at any point in the y direction may be calculated from the Poiseuille paraboloid,

$$u_y=2U\left(1-\frac{r^2}{R^2}\right),\ R=\text{inlet radius},\ -R\le r\le R \tag{6}$$

Original chamber

The original chamber has a flow angle of 90° to the sensors and exhibits poor flow characteristics; Fig. 7 shows the velocity map as a greyscale image. The lighter shading represents higher velocity, arrows also show velocity direction and magnitude. Flow analysis shows that 55% of the fluid flows in the channels to the sides of the sensors, only 45% of the flow is over the sensors; with the exception of the front face of the first sensor. This flow is relatively slow so that the refresh rate of species is very low, and this would produce poor sensor response. The sensors do not receive equal concentrations of species and due to the serial layout there is a lag between sensor responses. Sensor response is therefore position and flow rate related.

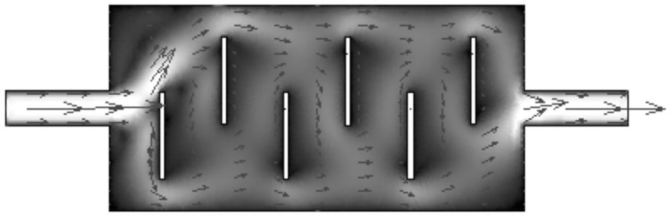

Fig. 7 Velocity profile in original chamber

Flow cell

Sensor responses at 90°

The flow cell with the sensors at 90° to the flow gives a serial sensor layout. Figure 8 shows the pressure distribution as the shading map (lighter shade is higher pressure),

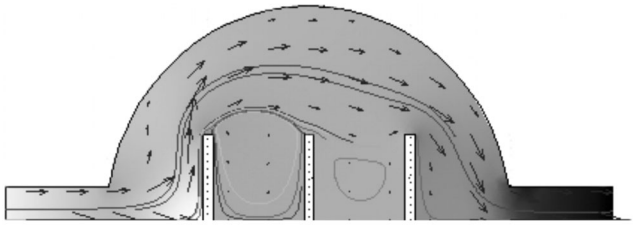

Fig. 8 Flow cell with sensors at 90° to flow

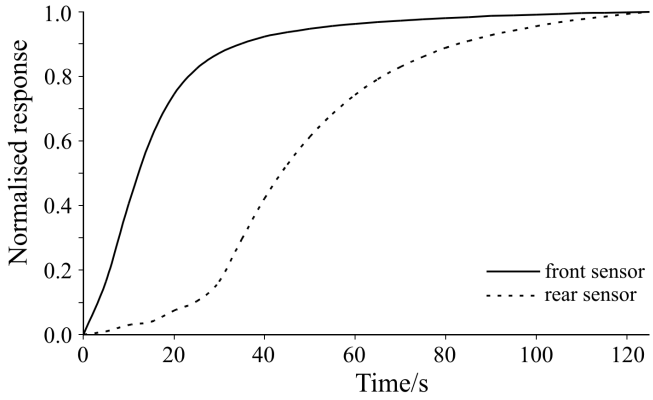

Fig. 9 Sensor responses at 90° to flow in flow cell (no baffle)

velocity vectors as arrows (direction and magnitude) and flow as lines. The pressure distribution is uneven with a large pressure head on the inlet face of the first sensor; the reference and rear sensor are at lower pressures with the outlet face of the rear sensor at the lowest pressure. There is a poor refresh rate between the sensors due to recirculation zones coupled with small velocities. The result is uneven sensor response as shown in Fig. 9. The front sensor responds rapidly to the incoming species whilst the rear sensor has a distinct lag, in part due to the refresh time of the chamber. The relatively long refresh time means that there is not a step change in the species concentration. Sensor response is position dependent.

Sensor responses at 0°

The flow for the sensors at 0° is shown in Fig. 10 and the sensor response for this in Fig. 11. There is an improvement over the 90° situation; the sensors now are in parallel and respond simultaneously to the incoming species. The pressure distribution is even over the sensors. The centre QCM has more flow over it than the outer two sensors. This is not ideal, the outer side of the sensors are not exposed to the full flow and therefore respond less rapidly than the ideal case. There is a slight lag for both sensors due to the refresh time of the chamber and the corresponding time for the species concentration to reach the outer faces of the sensors.

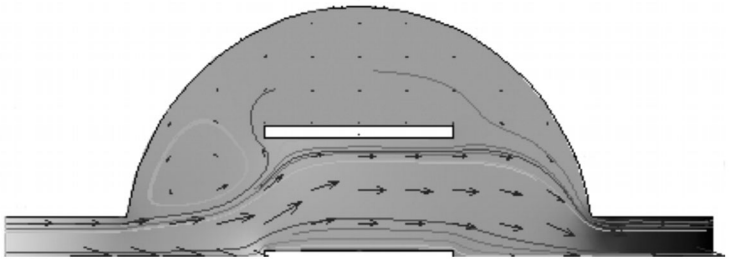

Fig. 10 Flow cell with sensors at 0° to flow

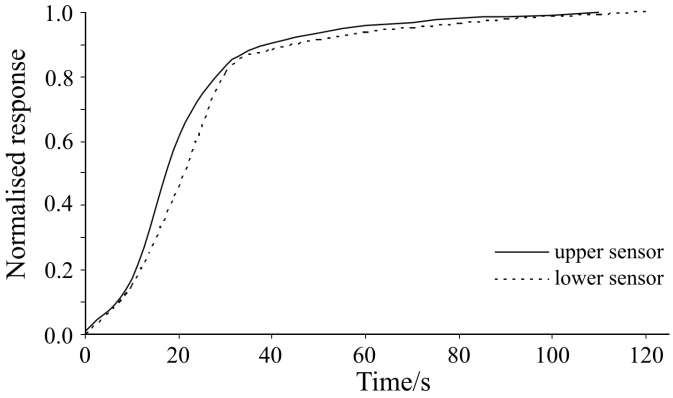

Fig. 11 Sensor responses with sensors at 0° to flow in flow cell (no baffle)

Sensor responses at 0° with baffle

The flow cell with the sensors at 0° to the flow and a set of baffle plates to diffuse the flow as shown in Fig. 12 is a further improvement over the 0° solution. The pressure distribution is even over the sensors as is the flow. The velocity distribution is also even over both sides of the sensors with no recirculation zones. The entire chamber is filled with species evenly and quickly, and as a result the sensors respond simultaneously, and the response profile is almost identical as shown in Fig. 13.

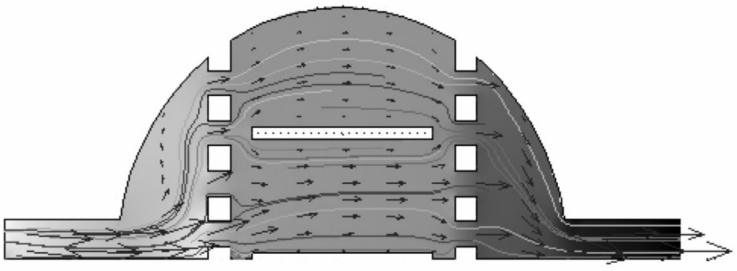

Fig. 12 Flow cell with baffles, sensors at 0° to flow

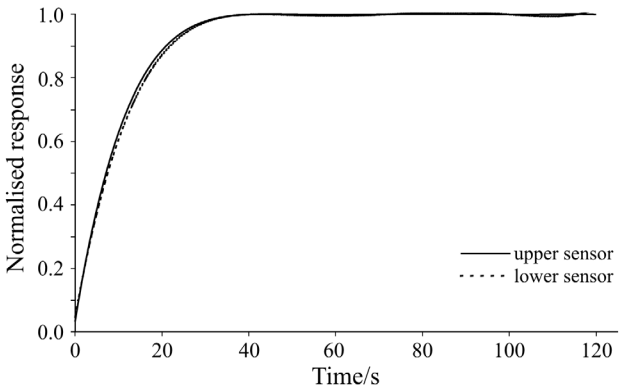

Fig. 13 Sensor responses with sensors at 0°to flow with baffle in flow cell

Dynamic concentration results

Figure 14 shows the CFD results for the surface concentration of an introduced species after one second. The lighter shading represents higher concentration of species. The original chamber (a) exhibits poor species concentration distribution; the front faces of the first three sensors are immersed in the new species whilst the rear three sensors have increasingly poor coverage. The test cell with the sensors at 90° to flow (b) shows the species hitting the front face of the front sensor then flowing around the reference and rear sensor. The sensors at 0° to flow (c) shows the species flowing cleanly over the reference, whilst only the inner faces of the sensors are covered by the species. For the sensors at 0° to the flow and a diffusing baffle plate (d) there is even concentration of the species over the sensors with the species almost filling the chamber. This satisfies the design criteria of a minimum refresh time, optimal flow angle over sensors of 0° with homogeneous flow, no recirculation zones, and all sensors exposed at the same time to the same concentration with no position related performance.

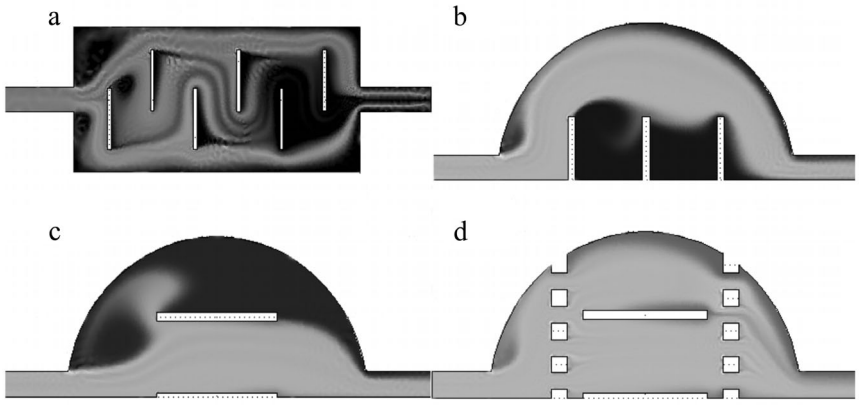

Fig. 14 Concentration at 1 s; a – original cell; b – 90°; c 0°; d – 0° with diffused flow

Optimised design

The design of the proposed flow chamber as shown in Fig. 15 incorporates all the features that have shown to be of benefit; the sensors are at 0° to the flow direction, so are in parallel. A baffle plate diffuses the flow evenly over all of the sensors; a second collects and combines the flow to outlet. All sensors receive the same flow at the same time; position related performance is therefore eliminated. The chamber, top cover and baffle plates will be constructed in stainless steel; the base of the chamber will be a sealed electronics board. Only inert, non-absorbent materials are to be used, eliminating any possible memory effects. There are seven QCMs inside the chamber; six are sensors, the central QCM acts as a reference. Assuming a chamber height of 15 mm, the volume is 13.11 cm^3. A 60 mL min^{-1} flow rate gives a chamber refresh time of 13.1 s which is not ideal but a reasonable compromise for the number of QCMs in the chamber and the flow rate.

Conclusions

A flow optimisation process using computational fluid dynamics was performed on the sensor chamber of an electronic nose. The models were related to actual performance of the sensors and flow visualisation studies. The simulations were developed using 2D CFD and took an inherited basic chamber design to an optimised chamber where sensor performance was much improved. The original chamber had several recirculation zones and 55% of the flow bypassed the sensors along the channels at the sides of the device.

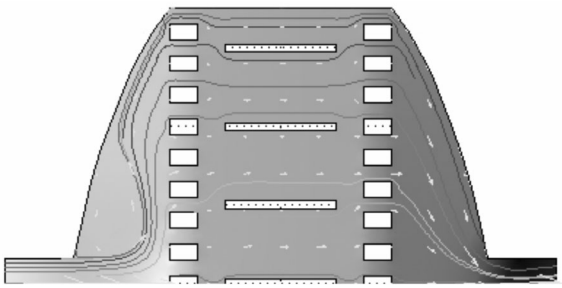

Fig. 15 Revised design, baffle and sensors at 0° in parallel

The test flow cell with the flow rate at 60 mL min^{-1}, a flow angle over the sensors of 0° and a diffusing baffle plate showed a clear improvement over the other configurations. The test sensors responded simultaneously with the same profile and achieve the same maximum value. From this optimum arrangement, a new flow chamber was designed and modelled which showed similar simulated characteristics to the optimum. The new design has a larger volume than the test cell as it contains seven QCMs, a reference and six sensors. The sensors will therefore not respond as rapidly as those in the test cell for the same flow rate.

References

1 T. Hamacher, J. Niess, P. Schulze Lammers, B. Diekmann and P. Boeker, Sens. Actuators B: Chemical, 95 (2003) 39.
2 R. Dutta, E. L. Hines, J. W. Gardner, K. R. Kashwan and M. Bhuyan, Sens. Actuators B: Chemical, 94 (2003) 228.
3 J. N. Barisci, G. G. Wallace, M. K. Andrews, A. C. Partridge and P. D. Harris, Sens. Actuators B: Chemical, 84 (2002) 228.
4 A. Guadarrama, J. A. Fernandez, M. Iniguez, J. Souto and J. A. de Saja, Sens. Actuators B: Chemical, 77 (2001) 401.
5 Q.-Y. Cai, J. Park, D. Heldsinger, M.-D. Hsieh and E. T. Zellers, Sens. Actuators B: Chemical, 62 (2000) 121.
6 P. McAlernon, J. M. Slater, P. Lowthian and M. Appleton, Analyst, 121 (1996) 743.
7 Z. Ali, D. James, S. M. Scott, W. T. O'Hare and F. J. Rowell, J. Therm. Anal. Cal., 71 (2003) 163.
8 Ding Hui, Liu Jun-hua and Shen Zhong-ru, Sens. Actuators B: Chemical, 96 (2003) 354.
9 M. Penza and G. Cassano, Sens. Actuators B: Chemical, 89 (2003) 269.
10 M. Holmberg, F. A. M. Davide, C. Di Natale, A. D'Amico, F. Winquist and I. Lundstrom, Sens. Actuators B: Chemical, 42 (1997) 185.
11 Z. Ali, D. James, S. M. Scott, W. T. O'Hare and F. J. Rowell, J. Therm. Anal. Cal., 71 (2003) 147.
12 D. James, S. M. Scott, W. T. O'Hare, Z. Ali, F. J. Rowell and T. I. Meas, Control, 26 (2004) 3.
13 M. Falcitelli, A. Benassi, F. Di Francesco, C. Domenici, L. Marano and G. Pioggia, Sens. Actuators B: Chemical, 85 (2002) 166.
14 G. Z. Sauerbrey, Z. Phys., 155 (1959) 206.
15 N. J. Freeman, I. P. May and D. J. Weir, J. Chem. Soc. Faraday Trans., 90 (1994) 751.